Annals of the Entomological Society of America Advance Access published July 15, 2015

Functional Anatomy of the Oral Region of the Potato Psyllid (Hemiptera: Psylloidea: Triozidae)

JOSEPH M. CICERO,[1,2,3] PHILIP A. STANSLY,[4] and JUDITH K. BROWN[1]

Ann. Entomol. Soc. Am. 1–19 (2015); DOI: 10.1093/aesa/sav059

ABSTRACT "*Candidatus* Liberibacter solanacearum", causal agent of zebra chip of potato and vein-greening of tomato, is prolific in tissues of the oral region of its vector, *Bactericera cockerelli* (Sulc). The region has, evolutionarily, reflexed under the head ("opisthognathy"), so that the mandibular stylets are ventral to the maxillary stylets, and both are directed posteriorly. The region includes the labium, furcasternum, and tentorium. The tentorium is a minute, crate-shaped, extremely complex endoskeletal apparatus consisting of preoral and postoral sections, with the primitive mouth in between. Except for certain prominent structures, its functional anatomy is poorly understood, and provisional (generic) terminology is needed to identify them. It is formed from several panel-shaped and rod-shaped invaginations of the preoral orifice. Panels divide the preoral section into four tissue blocks: hypopharynx, epipharynx, and two lateral blocks of questionable homological identity. Those between the hypopharynx and lateral blocks are fluted into "holsters." Holsters are extended into the postoral section as "loading sleeves." Together, both house the stylets. Stylet manipulation muscles are attached to them, not to the stylets themselves. Loading sleeves also function to guide presumptive stylets into their functional positions during a molt. Rods are located in the postoral section, and they form "ecdysial gaps" which also assist in molting. Stylets converge toward the preoral orifice, designed to interlock the maxillars and redirect the mandibulars to their flanks to form a "stylet bundle," and rotate the bundle 90° so that it can curve, about its most-bendable axis, into a cuticular pouch or "crumena" on exit.

KEY WORDS Liberibacter, oral region, stylet, tentorium, retortiform

The "potato psyllid," *Bactericera cockerelli* (Sulc) (Psylloidea: Triozidae) is considered to be the insect vector of the fastidious bacterium, "*Ca*. Liberibacter solanacearum" (CLso; Hansen *et al*. 2008; Liefting *et al.* 2008, 2009) that is associated with zebra chip of potato (Munyaneza *et al.* 2007, Crosslin *et al.* 2010), and vein-greening of tomato (Brown *et al.* 2010) diseases.

CLso has not yet been cultured, owing to its obligate nature. However, Ammar *et al.* (2011a, b) used high-specificity DNA probes and fluorescence *in situ* hybridization (FISH) to provide confirmatory evidence that the near-systemic bacteria in the Asian citrus psyllid, *Diaphorina citri* Kuwayama, is in fact "*Ca.* Liberibacter asiaticus" (CLas). J. M. C., T. W. Fisher and J. K. B. (unpublished data) used colloidal gold ISH to establish a morphotypic description of CLso which corresponds to, and therefore validates, bacteria referred to as CLso in potato psyllid-infested tomato (Liefting *et al.* 2009) and in Asian citrus psyllid-infested citrus phloem (Massonie *et al.* 1976, Bove 2006, Brlansky and Rogers 2007, Gottwald *et al.* 2007).

The present article is a morphological and functional elucidation of the oral region, launched with the discovery of morphotypic bacteria, profusely distributed in many tissues of this area that cannot be adequately identified. This elucidation will serve as the reference needed for a companion paper which details that distribution.

A comprehensive study of the literature revealed that prior works on the anatomy of the oral region are largely derived from the classical goal of associating internal and external cuticles with the primitive, orthopteroid condition, and developing a system of terminology that is based on the drawing of homologies (Snodgrass 1935, Duporte 1962, Singh 1971). The complications created using the homological approach interfered with our goal to produce a functional interpretation of the oral region for broader audiences. Functional genomics databases (transcriptomes) and proteomic resources that can be used to develop corresponding molecular and cellular hypotheses toward identifying key psyllid–CLso/CLas effectors that mediate transmission processes necessarily require a commensurate understanding in functional anatomy that is accessible to nonphylogenetic, nonanatomical researchers.

Comparative, homological anatomy is a very important school of thought, but, with the exception of

[1] School of Plant Sciences, University of Arizona, 303 Forbes Hall, Tucson, AZ 85721.
[2] Current address: Department of Entomology and Nematology, University of Florida IFAS, Steinmetz Hall, 1881 Natural Area Dr., Gainesville, FL 32611.
[3] Corresponding author, email: joecic@yahoo.com.
[4] University of Florida IFAS, Southwest Florida Research & Education Center, 2685 State Rd. 29 North, Immokalee, FL 34142.

certain well-known, well-accepted terms, it will not be held in subscription here. Instead, a provisional set of terms that connote location and function will be used where needed. Lastly, in this article, the deprecated term "homoptera" will be used throughout, as is relevant, to refer specifically to information published during the timeframe when homopterans were recognized as a separate Order.

Materials and Methods

Psyllid Colonies. Infected ($CLso^{\oplus}$) adult potato psyllids were obtained from infested tomato plants in Snowflake, AZ, during 2004, whereas uninfected ($CLso^{\ominus}$) adult potato psyllids were obtained that same year from greenhouse tomato plants in Willcox, AZ. Additional $CLso^{\ominus}$ colonies were obtained from potato fields in Hermiston, OR, and from the Yakima Agricultural Research Laboratory, Wapato, WA. Colonies were reared in separate insectaries on tomato plants placed in Bug Dorms (BioQuip Products, Rancho Dominguez, CA), and maintained at 22–24°C with a photoperiod of 12h:12h (L:D) cycle at the laboratory at The University of Arizona, Tucson, AZ.

Psyllid cultures were tested periodically to confirm presence or absence of CLso using CLso-specific 16S rRNA primers that amplify the OA2 (Liefting *et al.* 2008) and O12C (Jagoueix *et al.* 1996) genes, to produce a PCR product of 1,160 base pairs in size (data not shown).

Instrumentation. Hitachi S-3400N SEM, Phillips CM-12 TEM, JEOL 100CX II TEM (Tokyo, Japan), Axiophot compound microscope (Carl Zeiss, Thornwood, NY), Nikon SMZ-U (Melville, NY), and Olympus dissecting microscopes (Center Valley, PA), and LKB 2128 Ultratome 5 microtome were used.

Specimen Processing. Comparative analysis of transmission (TEM), scanning (SEM), and light micrographs was necessary to elucidate the oral region. For TEM, live, randomly collected $CLso^{\oplus}$ and $CLso^{\ominus}$ psyllids ($n = 9$, 12) were glued, dorsum down, to thumbtacks embedded in a paraffin-filled, plastic microwatchglass (Orach Machine Shop Service, Tucson, AZ), submerged in water, and stripped of any adhering bubbles with ducosate sodium (Aerosol OT, a wetting agent, Sigma-Aldrich, St. Louis, MO). After rinsing and submerging in 4% formaldehyde, 0.5% glutaraldehyde in 0.01 M Na^{+}–K^{+} phosphate buffered saline (PBS, Sambrook *et al.* 1989), pH 7.75, cuts were made with a razor blade as needed for the desired results. For identification of tissues associated with the stylets, cuts were made through the head along the lateral margins of the rostrum, and the surrounding structure of the head was pushed back, so that hemolymph, adipose material, and other obstructions would leach away. For Z-series section libraries of the oral region, specimens were cut transversely across the metathorax. Legs, antennae, and labial stylets were then carefully cut away. Fixation continued overnight, followed by rinsing with PBS. Some specimens were poststained with 1% osmium tetroxide (OsO_4) 20 min. Excisions of the tentorium were lifted out of the head, and, with half-bodies, moved through ethanol dehydration and LR White (Electron Microscopy Sciences, Hatfield, PA) infiltration series (25%, 50%, 75%, 95% overnight, 100% 3 h, then 25% LR White 6 h). Half-bodies were then put in separate vials for further infiltration, as it was discovered that LR White has the tendency to autopolymerize with more than one specimen. Infiltration continued in 75% LR White overnight, followed by 100% 6 h, and polymerization overnight at 52°C.

For light microscopy ($n = 8$), the oral region was dissected as a unit from the head in PBS. Specimens were transferred to fixative and processed as above. The graded ethanol series was expanded to 12.5, 25, 37.5, 50, 67.5, 75, 95% to minimize turbidity that causes entangling. Specimens were transferred to a well slide and photographed.

For SEM, the body was cut transversely across the pterothorax, and one lot of anterior halves ($n = 7$) was digested in *Bacillus* sp. protease (Sigma) overnight at room temperature, then cleared with xylenes overnight, rinsed in ethanol, dried in hexamethyldisilazane (HMDS), and mounted. Head exocuticle was pulled away from the inner oral region before sputter coating to reveal the oral endoskeleton. A second lot ($n = 6$) was digested in 1M potassium hydroxide (KOH) overnight at 42°C, rinsed in water, dried in the expanded ethanol series followed by HMDS, mounted, opened for viewing, and then sputter coated. Digested specimens were compared with TEM micrographs for indications that cuticle with low chitin content might have been stripped away, confusing interpretations.

Last instar exuviae were used to assist in interpretation of adult structures. Leaf surfaces infested with $CLso^{\ominus}$ potato psyllids were scanned continuously for pharate adults at the point of ecdysis so that fresh exuviae could be collected ($n = 9$) into water immediately upon emergence, followed by dehydration in ethanol and HMDS, and mounting on stubs. Dorsal exuvial halves were then removed, or folded over, to expose the exuvial tentorium for sputter coating.

Results

All figures are of adults unless indicated to be last instar exuviae. Identifiable structures were few in number relative to those that were unidentifiable. Identifiable structures included the tentorium, hypopharynx, cibarium, pharynx, esophagus, salivary pump, and brain.

The locations of characters elucidated in this article are described from the perspective of the viewer. For example, "inner dorsal" refers to the dorsal-most aspect of a structure when viewed through a cut-away of tissues dorsal to it. Example—Figures 1Bb and 2Aa point to inner dorsal views of the rostrum.

Mouthparts Were Directed Posteriorly. As with certain other homoptera (e.g., cicadas, sharpshooters), the whole of the primitively anterior section of the potato psyllid head was, evolutionarily, "bent under" or "ventralized," that is, shifted from an anterior direction ("prognathy"), to a posterior direction ("opisthognathy"; Fig. 3A and B). Correspondingly, the labium was

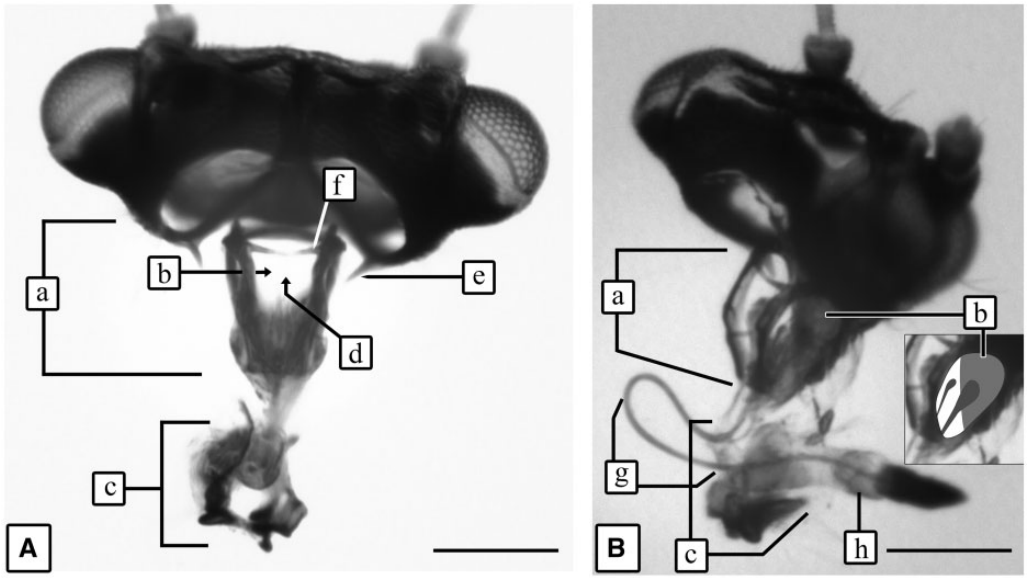

Fig. 1. Uninfected. Light micrographs of head and tentorium of two adults, cleared with KOH. Lines = 200 μ. **(A)** Dorsal view of head and tentorium. **(B)** Dorsolateral view. **(a)** Tentorium. **(b)** Lateral fenestration. In (B), stylet bases and the inner dorsal aspect of the rostral cuticle can be seen through this fenestration as clarified in right inset. **(c)** Furcasternum. **(d)** Dorsal fenestration. **(e)** Articulation spur. **(f)** Cross-bar. Partially dissolved. **(g)** Crumenal loop of stylet bundle. Crumenal sac had dissolved, but the stylet path was preserved. **(h)** Labium.

displaced posteriorly so that it protruded, in the ventral direction, as a shaft (the rostrum of Hamilton 1981), from a group of small, supporting sclerites, the "furcasternum," between the procoxae (Fig. 1Ac and Bc, h). The external, ventral aspect of the ventralized portion of the head is herein referred to as the "rostrum" (variously the consolidations of the clypeus, postclypeus, anteclypeus, and labrum of classical authors). The "oral region," then, extended from the anterior face of the rostrum (Fig. 2Bi) to the furcasternum.

With this change in head attitude, the stylet pairs (setae or bristles of classical authors), issued from the interior of the oral region to the exterior in a posterior direction, and the orientation of their bases relative to each other was reversed, with the mandibular stylets ("mandibulars") ventral to the maxillary stylets ("maxillars").

Mouthpart Anatomy Was Mostly Contained in a Quadrate Arrangement of Invaginations of the Exoskeleton That Fashioned the Tentorium. The tentorium was a crate-shaped (Hamilton 1981) arrangement of invaginations of the exoskeleton. All of its invaginations arose from, and were directed interiorly (anteriorly) from, the opening through which the stylets issued (the "preoral orifice"; Figs. 3Cg and 4Bl). For the purposes of this article, the interiors of all tentorial invaginations can be called "corridors" or "hollows" (collectively the "buccal cavity" of Davidson 1914). The epicuticles of the invaginations faced their hollows, and the tissue-side of the invaginations was layered with the hypodermal cells that secreted the cuticle (Fig. 3C, inset). There were two types of invaginations—"rods" and "panels." Neither the rods nor the panels could be considered "sclerites," considering their complex shape and seamless continuity of their cuticle between functional components.

The "side-arms" and "cross-bar" (Fig. 3Co) were rod-shaped invaginations. The panels were broad, flat invaginations (Fig. 3C, inset). Because the panels were invaginations, each had inner and outer walls with a hollow in between them, and their respective walls ended anteriorly in a "crease" (Fig. 3Cm).

The tentorium provided a rigid framework and cuticular spatulae (Figs. 3Cn and 10Bg) needed for attachment of muscles that controlled movements of the stylet bases and that of the salivary pump and food pump (cibarium).

The Rostrum Served as the Only Exoskeletal Foundation for the Tentorium. The external surface of the rostrum was a convex, tear-shaped lobe (Fig. 2B), directly attached to the surrounding hard cuticle of the head. An arthrodial membrane, pleated in life, occurred posteriorly, at the tip (Fig. 5Ah), allowing for weak articulation. Apparently, a second, paired, articulation point occurred about two spurs on the head (Fig. 1Ae). The rostrum was composed of a single wall of cuticle. The double-walled panels were directly attached to its dorsal surface (Fig. 4Be). Ventrally (exteriorly), the rostral cuticle was seamless, that is, there were no clypeolabral demarcations or indications of panel attachment. None of the tentorium components were attached to any other part of the exoskeleton—the panels curved inward leaving hemocoelic space between them and the surrounding head cuticle—there were no external cuticular features associated with the lateral aspect of the tentorium that might assist in homology and identification.

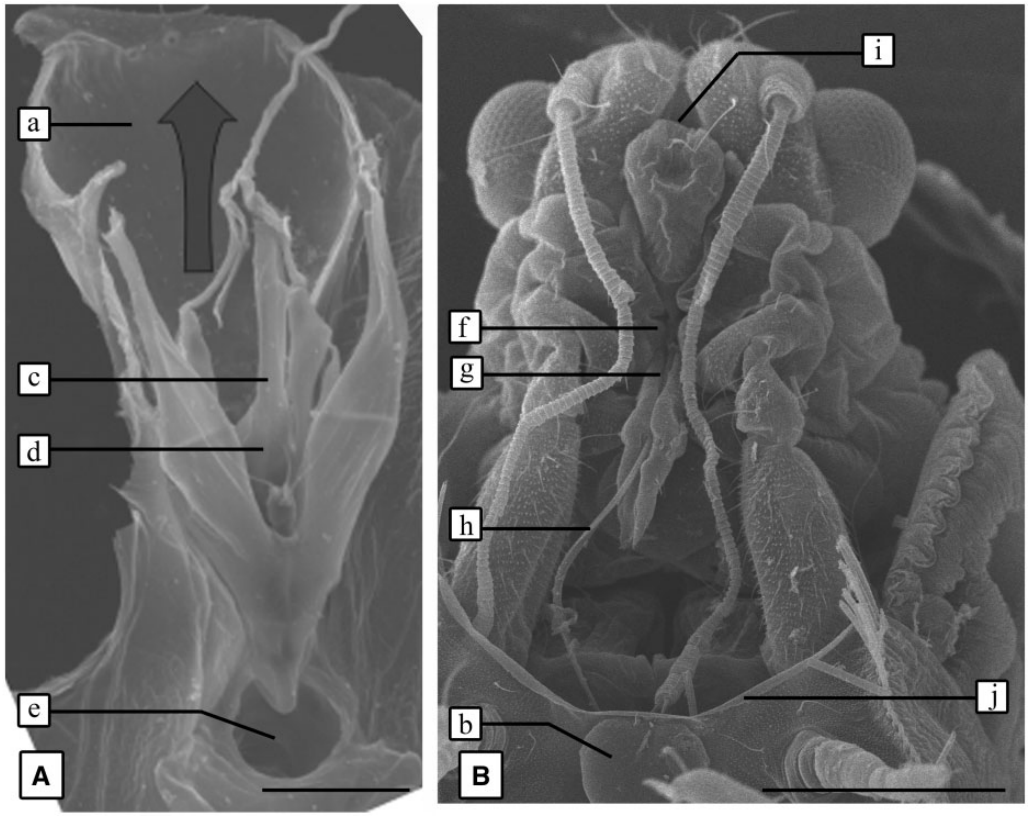

Fig. 2. Ecdysis of the adult potato psyllid. **(A)** Uninfected. Same specimen as Figure 5A. Oral region of last instar exuviae, inner dorsal view. Large arrow indicates path of lift of the presumptive head out of the exuviae. Line = 50 µ. **(B)** Infected. Ecdysing adult. Line = 250 µ. **(a)** Exuvial rostrum. Inner dorsal view. **(b)** Exuvial rostrum. Outer ventral view. **(c)** Pharynx. **(d)** Cibarium. **(e)** Inner dorsal view of labial interior. **(f)** Crumenal aperture. **(g)** Labial groove. **(h)** Stylet bundle. **(i)** Anterior face of rostrum is the anterior end of the tentorium. **(j)** Exuvial rupture.

The Tentorium Consisted of Preoral and Postoral Sections. The true, primitive, mouth was recessed into the head (Fig. 3Ds), dividing the tentorium into two sections, a posterior "preoral" section, and an anterior "postoral" section (Fig. 3Ci, j and Di, j). The preoral section included the panels and the first two of the food-stream lumina (the precibarium + cibarium of Backus and McLean 1982; the foregut (in part) of Ammar *et al.* 1994; the antecibarium + postcibarium of Harris *et al.* 1996; Fig. 3Dp, r). The preoral section also housed the internal aspect of each stylet, referred to herein as a "stylet base," as opposed to the external shaft (Fig. 3B).

The postoral section included the side-arms, crossbar, and the foregut or stomodeum—mouth + pharynx + esophagus (Fig. 3Ds, t, c). In sum, from posterior to anterior, the central, longitudinal hollow, or "primary oral invagination," started at the preoral orifice, and passed through the precibarium, then the cibarium, then the mouth, then the pharynx, and lastly the esophagus.

The Inward-Curved Panels and the Epipharynx Divided the Preoral Section Into Four Tissue Blocks. Two artifacts occurred with KOH treatment and SEM processing that may confuse the reader. With the dissolution of cells, the stylets shifted from their mesal position (compare Figs. 5Bs and 6Aa), and the thin cuticle in Figure 5Ak was lost.

It can be seen from Figure 5A that the panel walls transitioned into, respectively, different functional associations with different tissue blocks. As the literature was concerned with homologizing the blocks, drawing functional, referential names from it for the walls of each block was far too complicated. Perhaps the simplest alternative nomenclature is an acronym scheme, given in Table 1 and located in Figure 5A. The panels and hollows can be referred to by their associated walls. Examples—the paired LH–HW hollow flanked the salivary pump (Fig. 5Ab); the OL–LO panel curved inwardly around the dorsum of the lateral block (SEM—Fig. 5A, inset, curved arrow; TEM—Fig. 5A, curved arrow).

The structure pointed to in Figures 2Bi and 4Bu was only the exterior surface of the rostrum. Its internal, preoral half had a bridge (Fig. 5A, EW–n–EW), the "epipharynx," attached to it, which served as the ventral of the four tissue blocks. Its internal, postoral half was unmodified. The other three tissue blocks were: a dorsal block or "hypopharynx," and two muzzle-shaped "lateral blocks" (the maxillary stipital lobes of Hamilton

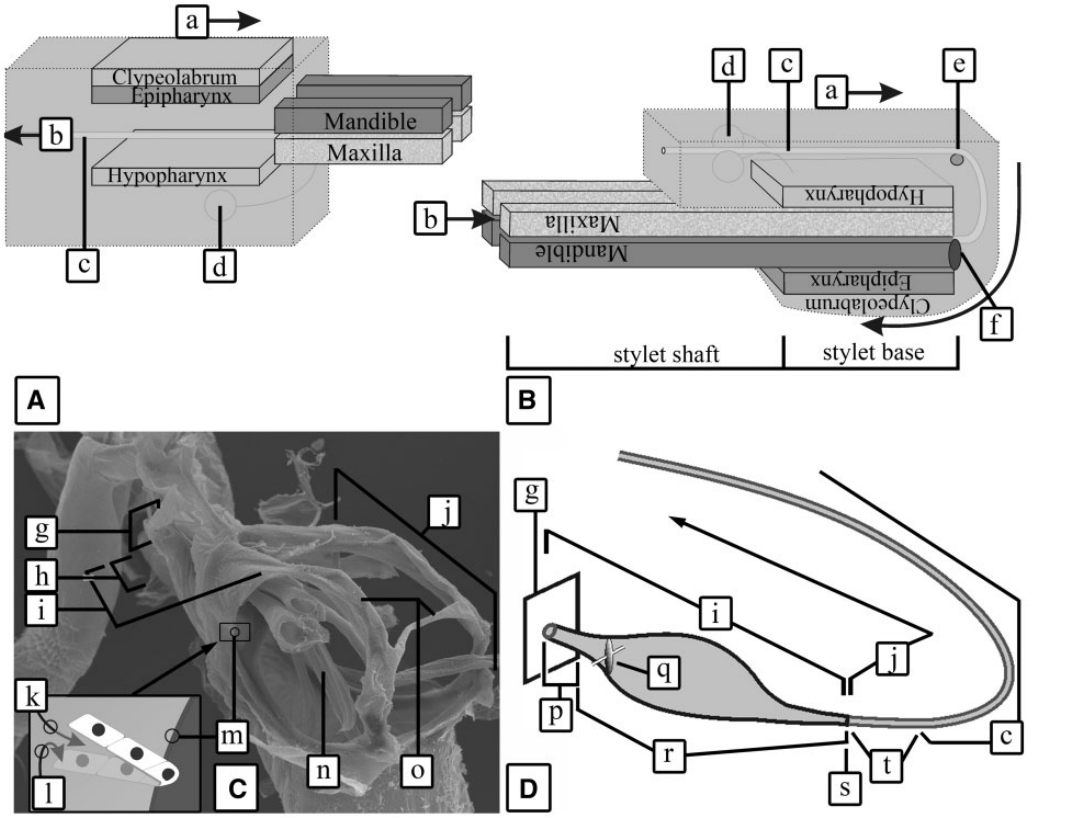

Fig. 3. Schematics. **(A–B)** Model for the evolution of opisthognathous mouthparts in the potato psyllid. **(A)** Primitive, prognathous arrangement such that mandibulars are dorsal to the maxillars, and both are directed anteriorly. **(B)** Derived, opisthognathous condition. Curved arrow indicates the evolutionary underturning of the mouthpart complex such that mandibulars are ventral to maxillars, and both are directed posteriorly. **(C)** Basic details of Figure 4B. Inset shows cells wrapping around crease of double-walled panel. **(D)** Basic details of the primary oral invagination. **(a)** Anterior direction of dorsum. **(b)** Direction of food-stream. **(c)** Esophagus. **(d)** Salivary gland. **(e)** Cross-bar. **(f)** Stylet regenerating cell assemblage. **(g)** Square inset locates the preoral orifice. **(h)** Posterior end of the tentorium. **(i)** Preoral section. **(j)** Foregut. **(k)** Hollow. **(l)** Epicuticle side. **(m)** The anterior edge of the panel is a crease. **(n)** Cuticular partitions. **(o)** Side-arm and cross-bar. **(p)** Precibarium. **(q)** Insert is meant to indicate that the preoral food-stream is formed by opposing concavities of hypopharynx and epipharynx. **(r)** Cibarium. **(s)** Mouth. **(t)** Pharynx.

1981; the laminae maxillaries of Weber 1929; the maxillary sclerite of Davidson 1914; Fig. 5Ad). The literature holds that the epipharynx is a modification, or lobe, on the inner surface of the labrum or clypeus, and that the hypopharynx is homologous to the grasshopper tongue. Both homological derivations are questionable for homoptera, but as they have been stable terms in homoptera, they are adopted here on that basis.

The panels formed the hypopharynx by curving inward, so that OL–LO transitioned into LH–HW (Fig. 5A). The ventral surface of the hypopharynx (Fig. 5Am) served as the dorsal surface of the preoral food-stream lumen (Fig. 5Af). The dorsal surface of the epipharynx (Fig. 5An), in turn, served as the ventral surface of that same lumen.

All four blocks were separated from each other by cuticle-lined hollows, but each was open to the anterior. That is, their internal tissues were continuous with those of the postoral section, indicated by locant (o) in Figure 5B. A small, unidentified block occurred in the anterior-most cross-section (Fig. 5Bt).

The Side-Arms Extended From the Dorsum of Each Lateral Tissue Block. The cross-section in Figure 5A was located posterior to the emergence of the side-arms (Fig. 5A inset). Anterior to this cross-section, each OL panel wall extended anteriorly into a rod to form a side-arm (Fig. 7C, OL). The continuous, paired OL–LO-to-LH–HW crease (Fig. 4Bo) had thick cuticle that made imprints (the anterior tentorial pits of classical authors) on their respective, collapsed, side-arms in dried specimens (Fig. 4Aa).

The side-arms spanned the longitudinal length of the postoral section (Fig. 4Bp), and were transversely connected to each other by one cross-bar (Fig. 4Bs; Supp. Fig. 2 [online only]). Just anterior to the cross-bar, the side-arms bent ventrally to become the dorsal halves of the "vertical-arms" (Fig. 4Bt). The ventral halves of the vertical-arms were the terminal ends of paired corrugations (Fig. 4Bq) that extended, on either

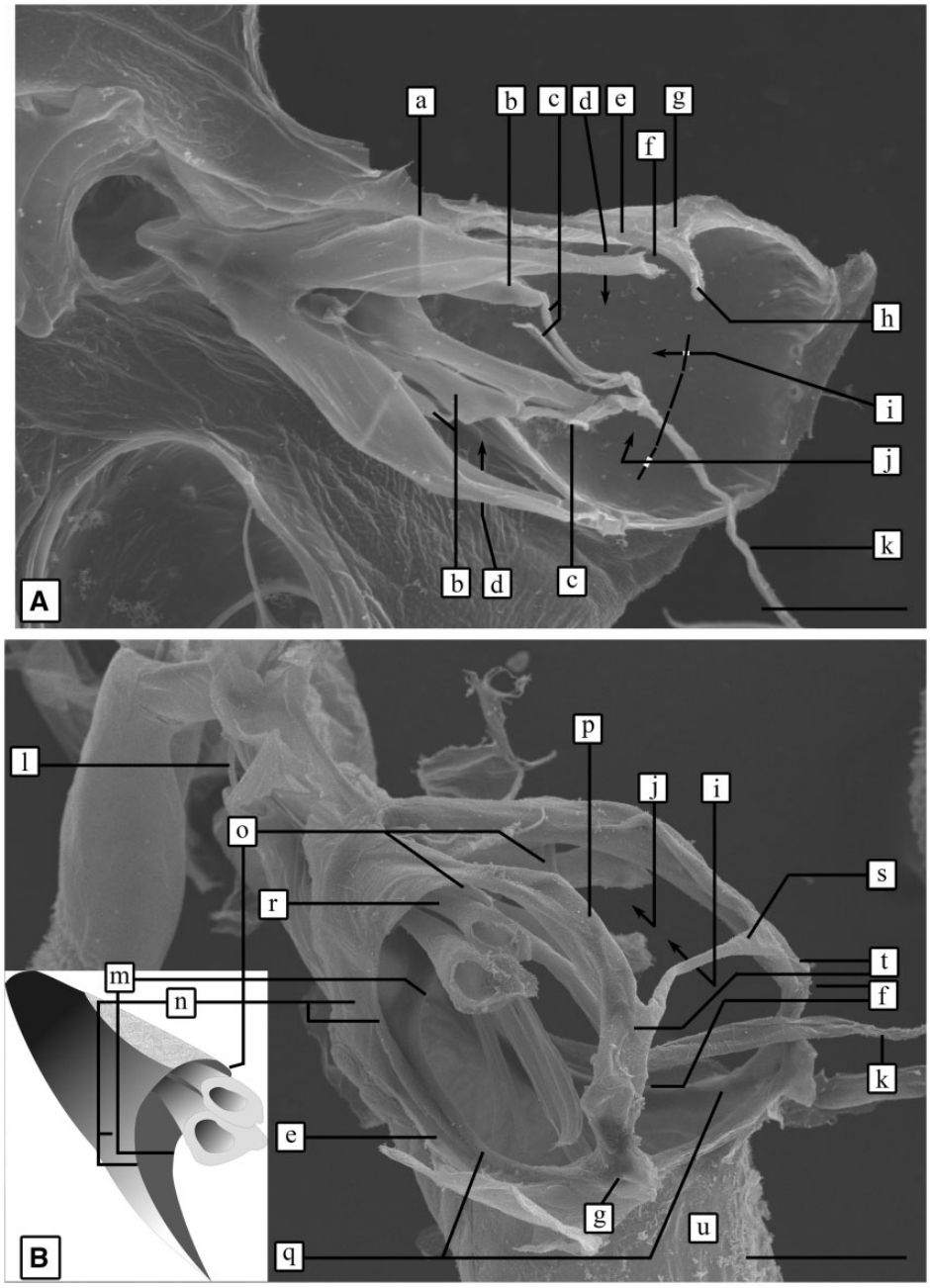

Fig. 4. SEM of the exuvial and adult tentoria. Lines = 50 µ. **(A)** Uninfected. Same specimen as in Figure 2A. Last instar exuvial tentorium. Dorsal view. **(B)** Infected. Adult tentorium, KOH cleared. Dorsolateral view. Inset—Isolation of the lateral block. Side-arm is removed. The hypopharynx–epipharynx opposition (Fig. 5Am, n) is not visible. **(a)** Imprint of underlying crease (o). **(b)** Exuvial stylet base inside loading sleeve (cf. Fig. 6Bk, l). **(c)** Atria. One of the pair broke away from its loading sleeve, the latter not visible in this micrograph. **(d)** Lateral fenestration. **(e)** Basolateral edge of rostrum. **(f)** Ecdysial gap. Open in (A), closed in (Bs). **(g)** Uplifted anterior rostral corner forms ventral half of vertical-arm. **(h)** Predigestion of exuvial cuticle removed the cross-bar (Bv), represented by the dotted line. **(i)** Anterior fenestration. **(j)** Dorsal fenestration. **(k)** Esophagus. Atria are tangled with it. **(l)** Stylet bundle, externally visible on exit from the preoral orifice. **(m)** Crease of the LE–EW panel. **(n)** OL panel wall. The OL–LO crease is also pointed to. **(o)** OL–LO tracks dorsally, curving over the stylet bases. **(p)** Side-arm emerges from OL. **(q)** The LE–EW crease continues anteriorly to vertical arm (g). **(r)** Maxillar. **(s)** Cross-bar. **(t)** Anterior end of side-arm bends to the dorsum, forming dorsal half of vertical-arm. **(u)** Anterior face of rostrum.

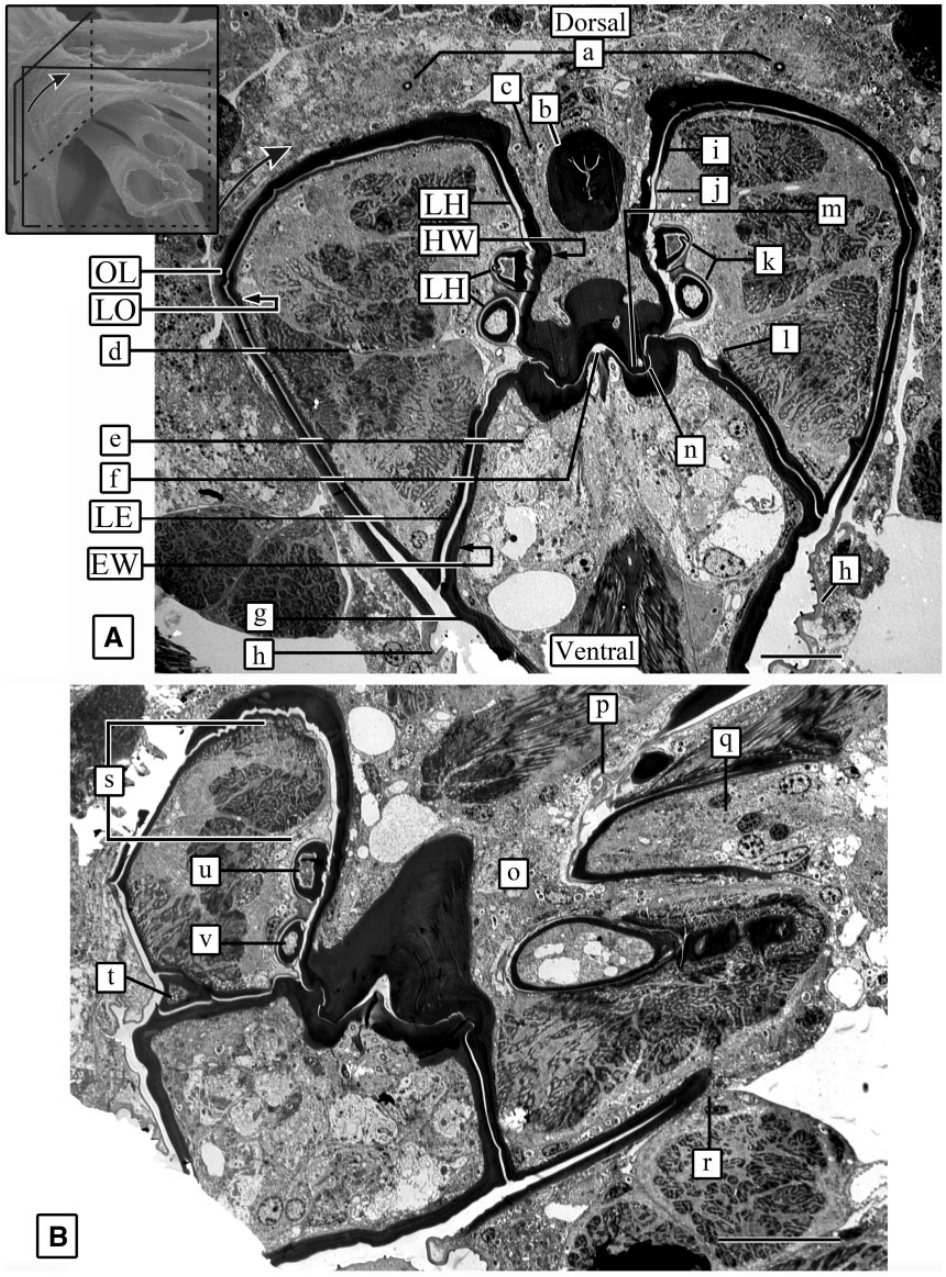

Fig. 5. Uninfected. The four tissue blocks of the tentorium. See Table 1 for panel abbreviations. Inset—Transverse and sagittal boxes correspond to locations of, respectively, (A) and (B). **(A)** Transverse cut of the preoral section. Curved arrows indicate that the OL–LO panel curves around to the dorsum and transitions into the LH–HW panel. Line = 10 µ. **(B)** Transsagittal section showing the preoral configuration of (A) on the left side, and the postoral configuration on the right side. Line = 2 µ. **(a)** Salivary ducts. **(b)** Salivary pump. **(c)** Cellular interior of hypopharynx. **(d)** Cellular interior of lateral block. **(e)** Cellular interior of epipharynx. **(f)** Primary oral invagination between (m) and (n). **(g)** Rostrum. **(h)** Pleated arthrodial membrane. **(i)** LO cuticle rounds the dorsum to become LH and thins at **(j)** to form **(k)**, a pair of half-tubes, or "stylet holsters." LH then thickens again at **(l)** to become LE and continues without participating in forming the primary oral invagination. **(m)** Ventral surface of hypopharynx. **(n)** Dorsal surface of epipharynx. **(o)** Postoral section, anterior to the creases that close the double-walled panels. Tissues from adjacent blocks have consolidated. **(p)** LH pinches away from HW to form the loading sleeve. **(q)** Cell-filled hollow of the maxillar base. **(r)** Crease. **(s)** Distance between maxillar and dorsum of lateral block. **(t)** Unidentified tissue block. **(u)** Maxillar. **(v)** Mandibular.

side, from the crease of the paired, opposing LE–EW panels to the uplifted anterior rostral corners (Fig. 4Ag and Bg).

Table 1. Legend for the walls of the four tentorial tissue blocks

Abbr.	Description
LE	Lateral block wall that opposes the epipharynx
EW	Epipharyngeal wall
LH	Lateral block wall that opposes the hypopharynx
HW	Hypopharyngeal wall
OL	Outer wall that opposes the lateral block
LO	Lateral block wall that opposes the outer wall

The Windows ("Fenestrations") Allowed for Structures to Pass From Inside the Tentorium to the Outside and Vice-Versa. The postoral section was bounded laterally, anteriorly, and dorsally by, respectively, the "lateral," "anterior," and "dorsal" fenestrations (Fig. 4Ad, i, j). The flats of the stylet bases occurred at the lateral fenestrations. Cerebral tissue intruded through the dorsal fenestration (Fig. 8Ah; Supp. Fig. 2c [online only]). The esophagus passed anteriorly, through the anterior fenestration, and was then redirected to the posterior (Fig. 3Dc) to pass through the thorax to the midgut. As a result of ecdysis, the exuvial esophagus (Fig. 4Ak) was redirected to the anterior during the teneral adult's lift (Fig. 2A arrow) out of the exuviae.

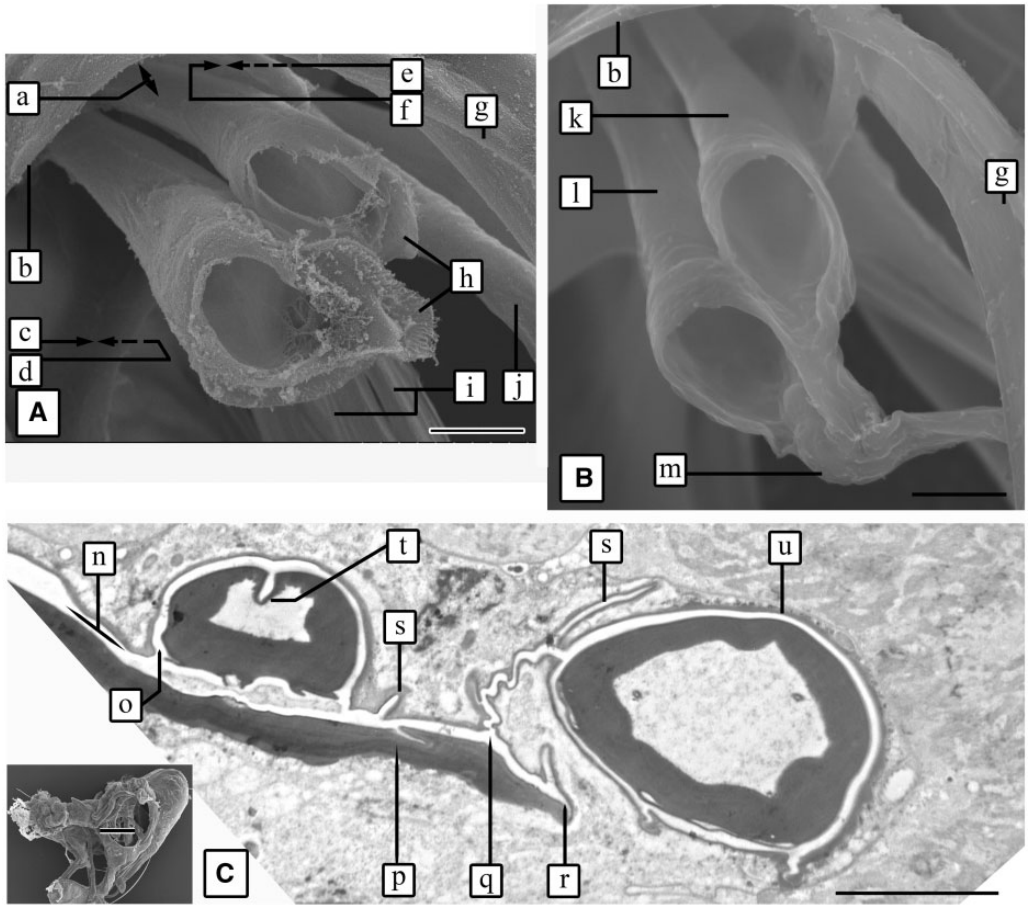

Fig. 6. Stylet bases. Lines = 10 µ. **(A)** Infected. Magnification of stylet bases in Figure 4B. Cleared with KOH. **(B)** Uninfected. Last instar exuvial stylet bases, not cleared in KOH. **(C)** Infected. Cross-section near the anterior end of the preoral section. Cross-section is at an angle such that the maxillar is in its holster, while the mandibular is in its loading sleeve. Inset, from Figure 8C, showing location of cross-section. Line = 5 µ. **(a)** KOH removed the cells, causing a repositioning of stylet bases up against the inner dorsum of the lateral block (compare with Fig. 5Bs). **(b)** OL–LO crease. **(c)** LE. **(d)** EW. **(e)** HW. **(f)** LH. **(g)** Side-arm. **(h)** Auricles. **(i)** Cuticular spatulae. **(j)** Pharynx-esophagus. **(k)** Loading sleeve. Maxillar is inside. **(l)** Loading sleeve. Mandibular is inside. **(m)** Extensions of the loading sleeves. Interpreted as the atrial walls that unraveled, during ecdysis, from their functional, pleated arrangement as cushions (cf. Figs. 7Do and 8B), and ripped open to expose the stylet cores. **(n)** Hollow between LH and HW, continuous with the outside of the body. **(o)** Hollow invaginates to holster the maxillar. **(p)** Thick cuticle of HW. **(q)** Pinch (cf. Fig. 7Be, f). **(r)** Crease. **(s)** Spurious branches in the hollows may facilitate flexibility during stylet manipulation. **(t)** Thin, invaginated epicuticular sleeve in outer lateral surface of maxillar. **(u)** Loading sleeve with mandibular inside.

The Tentorium Was Also Designed to Accommodate Ecdysis. Elucidation of the adult tentorium necessitated elucidation of the last instar exuvial tentorium. In the adult, the cross-bar was intact, but in the exuviae, the cross-bar was absent or attenuated in the center (Fig. 4Ah). In the adult, the contact between the dorsal and ventral halves of the vertical-arms (the posterior tentorial pits of classical authors) was closed (Fig. 4Bf), but in the exuviae, it was open, that is, the dorsal and ventral halves were attenuated away from each other, forming "ecdysial gaps" (Fig. 4Af) as a consequence of the lifting out of the presumptive adult head during ecdysis.

The LH Panel Wall Was Functionally Differentiated. The LH panel wall can be tracked in Figure 5A, as follows. The thick cuticle of LO rounded the lateral block dorsally to become LH. At locant (i), the LH cuticle thinned and diverged away from HW as a flexible "half-tube" which, backed by the HW wall, housed the stylets. The LH cuticle thickened at locant (l) to become the LE wall. The paired, opposing LE–EW panels continued ventrally without involvement in formation of the primary oral orifice (locant (f)).

The Left and Right Stylet Pairs Converged, in a Posterior Direction, to the Preoral Orifice. The stylet bases were cone-shaped—elliptical in cross-section and attenuating in diameter posteriorly. The stylet pairs were widely separate from each other at the flat of their bases, and gradually angled toward the midline, to the preoral orifice, in association with the narrowing of the dorsal, ventral, and lateral blocks.

The greatest complexity of the tentorium was observed at the posterior end of the preoral section (Fig. 3Ch), where tissues and cuticles were highly modified to accommodate the tightly sealed convergence of stylets, preoral foodstream, and the efferent salivary stream. An efferent salivary duct was not searched for in this study.

The Preoral Section Contained the Stylet Holsters. As mentioned above, the cuticle of the LH panel wall was thinned and underwent a secondary invagination outwardly, away from the tentorial midline (Fig. 5Ak), to form half-tubes. These, backed by the thick HW cuticle (Fig. 6Cp; the "hypopharyngeal wings" of various authors), formed the stylet "holsters" (the "stylet pouches" of classical authors).

Figures 4, 5, and 6 showed different features involved in housing the stylets. These features are graphically merged into a composite diagram (Fig. 7). The opposition of the hypopharynx and epipharynx was not visible in SEM specimens, and interpreted to be recessed into the preoral section.

The Postoral Section Contained the Loading Sleeves. Near the LH–HW crease, which marked the anterior end of the preoral section, the thin cuticle of each holster's LH panel wall was pinched away from the HW backing (Figs. 5Bp, 6Cq, 7Be, f, and 8Ae), and continued into the postoral section to become a "loading sleeve" (Figs. 6Bk, l, Cu, and 7Bg, Cg), so named for its functional participation in stylet biogenesis (see Discussion). The space between the loading sleeves and the stylets was continuous with that of the holsters, and with the outside of the body (Fig. 6Cn). In Figure 4B, KOH removed both the loading sleeve cuticle and the holster cuticle, exposing the true stylet cuticle and an "auricle" (Fig. 6Ah).

Exuvial Loading Sleeves Transitioned into Atria. In both adult and exuviae, loading sleeves were seen to invest the stylets (Figs. 4Ab and 6Bk, l, Cu). In exuviae only, another cylinder, continuous with the loading sleeves, extended beyond the flat of the stylet bases (Figs. 4Ac and 6Bm) and tangled with the exuvial esophagus. These extensions are interpreted to be the "atria" of the stylet regeneration organs (the "retortiform organs" of classical authors; see Discussion). The atria pointed to in Figure 6Bm collapsed at their junction with the loading sleeves during the exuvial process, exposing the hollow stylet cores.

A Cuticular Cushion Occurred at the Extreme Base of the Loading Sleeve. In adults, there occurred a "cushion" of thin, loosely involuted, cuticular infoldings (Figs. 7Do and 8B) in a pocket at the extreme base of each stylet, in the hollow between the inner (epicuticular) loading sleeve wall and the stylet epicuticle, These were the only sections of cuticle observed in which an underlying layer of cells was absent.

Basal Maxillar Morphology Was Strongly, Gradually, Longitudinally Stratified. Four morphological features of the maxillar base were observed. 1) The core. The maxillar, like the mandibular, had a cell-filled core (Figs. 6C and 8Ak), but it extended no further posteriorly than the preoral orifice. On exit from the preoral orifice, its interior was solid, in contrast to that of the mandibular, which retained its cell-filled core (Fig. 9Bl). 2) The longitudinal ridges. The ridges were absent in the postoral section, and incipient on entry into the preoral section (Fig. 8Af, k). The ridges took on gradual definition as they transitioned toward the preoral orifice, and the spaces between them too, took on gradual definition as grooves. Five ridges occurred on both maxillars in the preoral section (Fig. 10C, D). 3) The flattening of width. A flattening of width occurred during this transition, from an elongate oval cross-sectional shape in the postoral section (Fig. 4Br), to a flat, rectangular cross-sectional shape at the preoral orifice (Fig. 9A). 4) The "sleeved" epicuticle. On entry into the preoral section, the maxillar epicuticle pinched inwardly into a "sleeve." In cross-sections through the preoral section (Figs. 6Ct and 10Do), the sleeve occurred on the outer lateral surface, and was looped into the interior. In cross-sections of the exit of the stylets from the preoral section, the sleeve occurred on one lateral end, and looped to the exterior (Fig. 9Ac, Bc).

The Salivary Canal Was Formed by the Failure of a Ridge to Fill its Opposing Groove. On exit from the preoral orifice, the maxillars were interlocked to form the food canal (Fig. 9Bk) and salivary canal (Fig. 9Bi). One longitudinal ridge completely filled its opposing groove (Fig. 9Bj), while the other, in developmental terms, failed to do so. It was only about half as tall, leaving a gap that constituted the salivary canal.

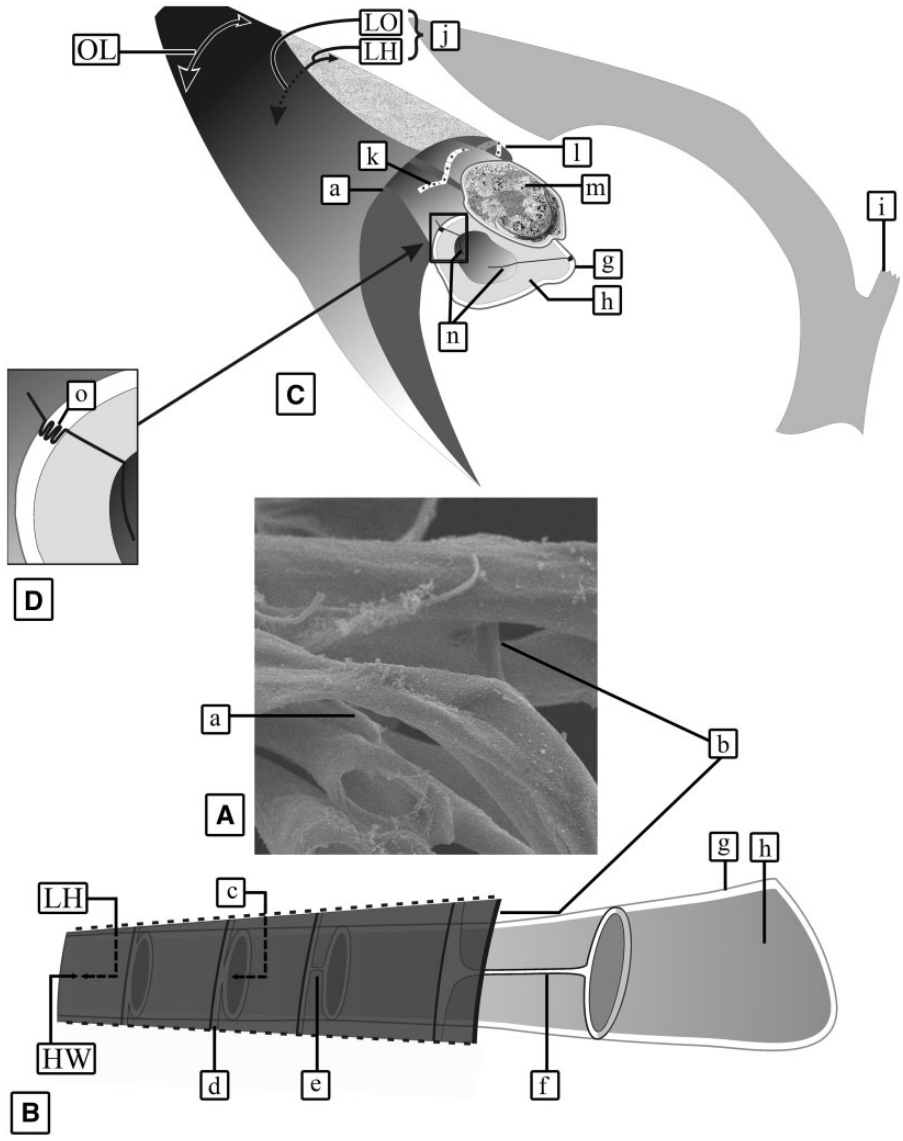

Fig. 7. Greater detail to Figure 4B. **(A)** Inset from Figure 4B. Serves as a pivotal figure about which (B), (C) and (D) can graphically represent its complex components. **(B)** Transition from holsters to loading sleeves. HW is in the foreground, LH and locant (c) are in the background. **(C)** Lateral block with samples of hypodermal cells. Curved arrows represent the curvature of the identified panel walls. The side-arm is considered an extension of the OL panel wall. **(D)** Closeup of cuticular continuity. (**a**) LO-OL crease in (**C**) is continuous with LH-HW crease in (**A**). Locant (**a**) in (**A**) points to the LH-HW crease on contralateral side of the graphic in (**B**). (**b**) LH–HW crease on contralateral side of (a). **(c)** Stylet inside holster. **(d)** Continuous hollow. **(e)** In life, LH pinches away from HW (cf. Figs. 5Bp, 6Cq and 8Ae). LH is mostly thin cuticle that is lost in (**A**) with KOH treatment. **(f)** In life, the pinch lengthens and continues along the loading sleeve. **(g)** Loading sleeve, lost with KOH treatment. **(h)** Stylet inside loading sleeve. **(i)** Cross-bar. **(j)** Lifting of the side-arm gives a dorsal view of the hollow and the epicuticle in transition from LO to LH (cf. Fig. 5A, arrows), otherwise hidden behind the OL panel wall. LO is underneath OL. **(k)** These cells secrete the thin holster cuticle of LH (cf. Fig. 5Ak). **(l)** Cells round the LH–HW crease. **(m)** Stylet endcap cells. **(n)** Cuticular continuity. **(o)** Cushion (cf. Fig. 8B).

Basal Mandibular Morphology Was Weakly, Gradually, Stratified Longitudinally. The mandibular transitioned from an elongate oval cross-sectional shape in the postoral section (Fig. 6Cu) to a semicircular cross-sectional shape in the preoral section (Figs. 9Ab and 10C, D). A pair of epicuticular sleeves appeared in the preoral section, as indicated in Figures 9Ab, Bb, and 10Dn.

Cross-sectional sampling indicated that the mandibular core remained uniformly ovate-cylindrical in shape, and cell-filled from the base to beyond exit from the head. Basally, the core had typical cellular inclusions

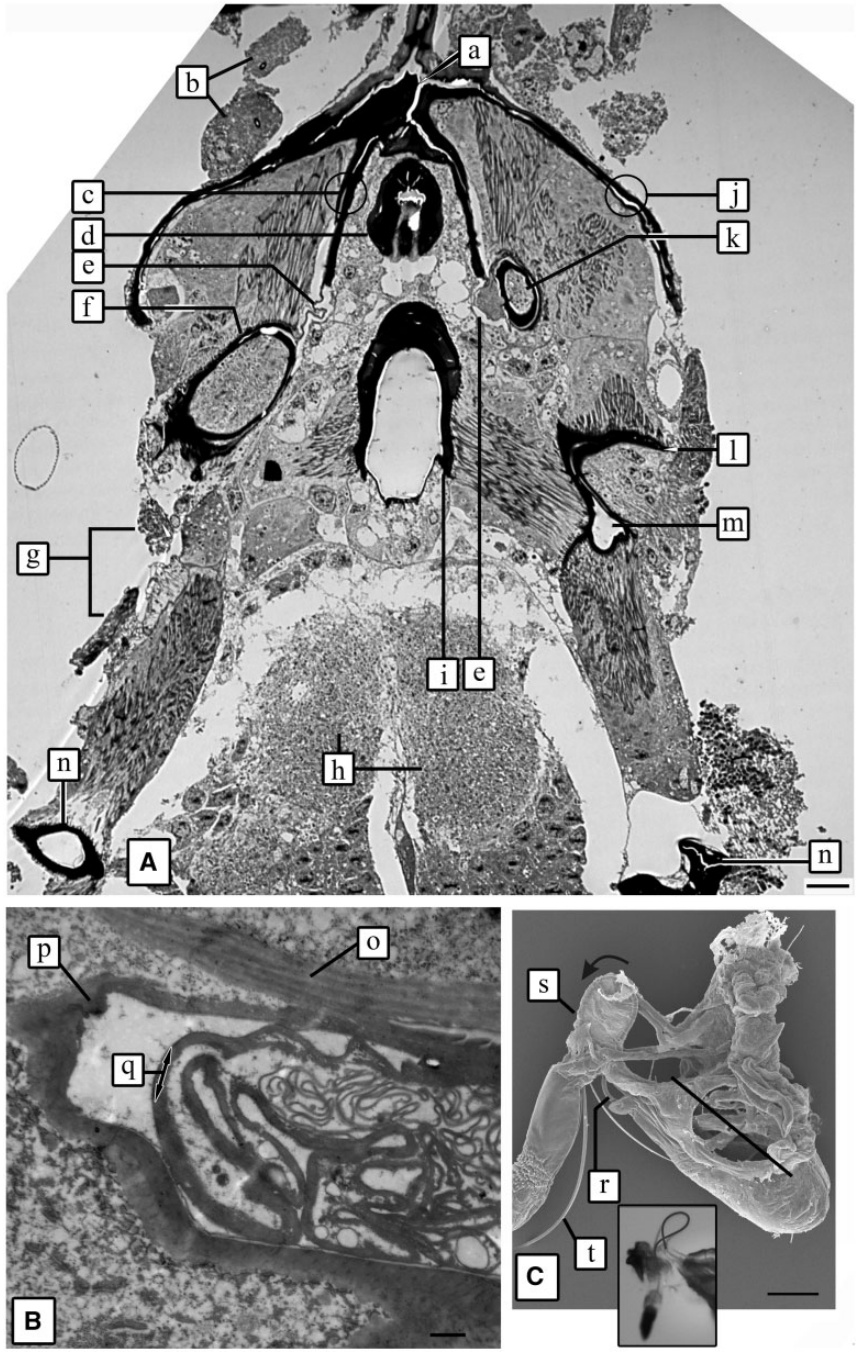

Fig. 8. Uninfected. **(A)** Frontosagittal section. Line = 10 µ. **(B)** Stylet base, showing a cushion of cuticular reams. Interpreted as the atrial walls (cf. Fig. 4Ac, 6Bm and Discussion). Line = 500 nm. **(C)** Uninfected. SEM, lateral view. Tentorium cleared with protease. Inset—From Figure 1B. An alternative looping, drawn in, was not observed in any specimen. Line = 50 µ. **(a)** Hollow near the posterior end of the demarcation between dorsal and lateral tissue blocks. **(b)** Salivary ducts. **(c)** LH–HW. **(d)** Salivary pump. **(e)** Thin cuticle of pinch (cf. Figs. 5Bp and 7Bf). **(f)** Cross-section of maxillar in the postoral section, inside its loading sleeve. **(g)** Location of mandibular, lost during microtomy. **(h)** Cerebral tissue (cf. Supp. Fig. 2c [online only]). **(i)** Cibarial pleat (Supp. Fig. 3Bf [online only]). **(j)** OL–LO. **(k)** Cross-section of maxillar in the preoral section. Longitudinal ridges are indicated. The loading sleeve and holster are in transition. **(l)** Diagonal cut through the flat of the mandibular base renders a crescent shape rather than a closed, oval shape. **(m)** Space between mandibular and loading sleeve. **(n)** Vertical arms. **(o)** Mandibular cuticle. **(p)** Pocket in the loading sleeve that houses the cushion. **(q)** Arrows indicate purported continuity of the cushion cuticle with adjacent cuticles. One direction leads to the loading sleeves, the other leads to the stylet base. **(r)** Exit of stylet bundle in a posterior direction. Stylet bundle exits the preoral orifice, rounds the crumena **(s)**, and, in life, enters into the labial furrow **(t)**, completing a 90° angle change in direction, from posterior to ventral.

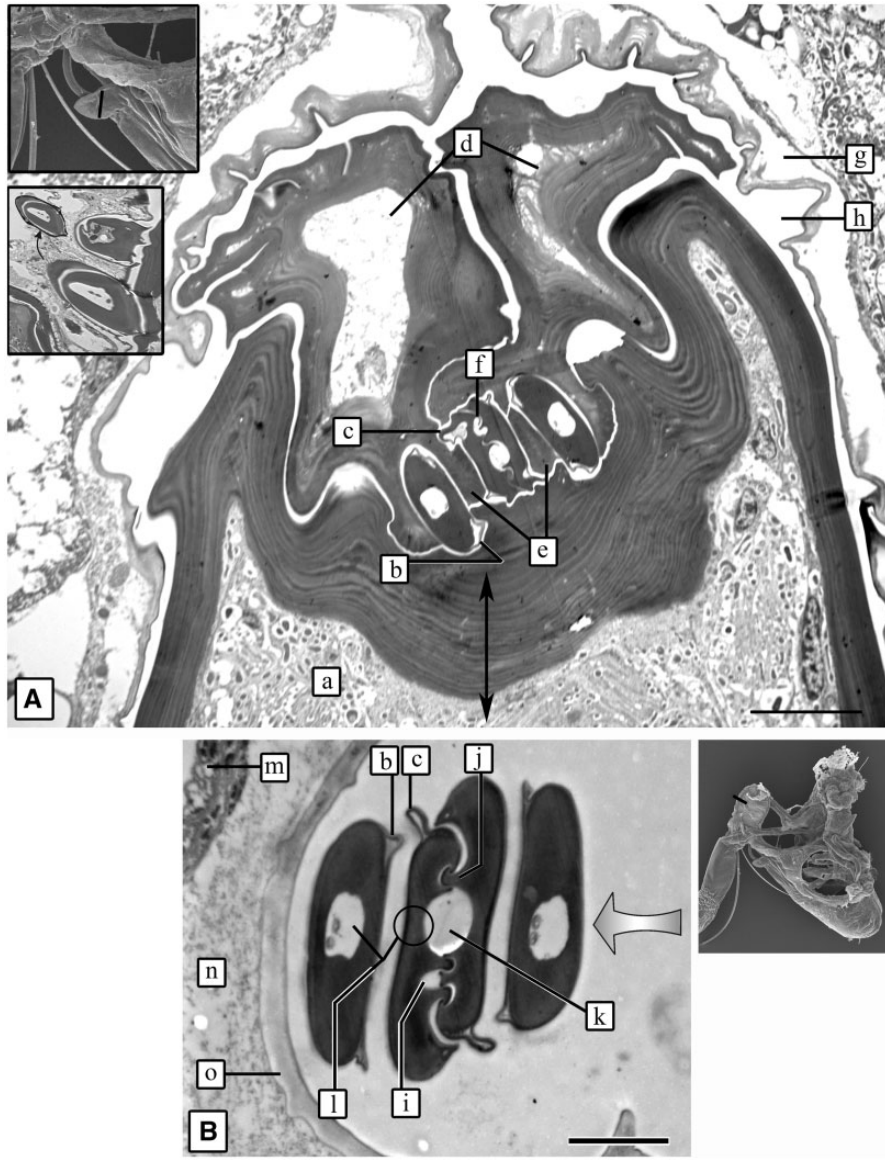

Fig. 9. Stylet bundle. Insets from Figure 8 show location of the cross-sections. **(A)** Infected. TEM of the stylet bundle near its exit from the preoral orifice. Double arrow—longitudinal midline. Note that all four stylets are laterolateral with respect to each other, and, collectively, angled relative to the midline. Lower left inset—from Figure 10C. Arrow indicates the rerouting of the mandibular so that it is lateral to its maxillar. Line = 10 µ. **(B)** Uninfected. Stylet bundle inside crumena. Arrow indicates that the stylet bundle curves about its most-bendable axis. Line = 2 µ. **(a)** Rostral apex. **(b)** Mandibular with sleeve. **(c)** Maxillar sleeve. **(d)** Apical extents of the lateral blocks interlocking with the rostral apex (a), and confining the stylet bundle. **(e)** Holster walls fit between stylet pairs (cf. Fig. 10Cj and Dp). The maxillars are interlocked, indicating that the hypopharynx does not extend this far posteriorly. **(f)** Salivary canal. **(g)** Artifactual separation of cells from cuticle. **(h)** Cuticular pleats (cf. Fig. 5Ah). **(i)** Salivary canal is formed by a maxillar ridge that is too short to fill its groove. **(j)** Opposing maxillar ridge is long enough to fill its groove. **(k)** Food canal. **(l)** Mandibular has a dendritic core. Maxillar has no core. **(m)** Crumenal hypodermis. **(n)** Crumenal procuticle. **(o)** Crumenal epicuticle.

(Fig. 8A, between l and m). More distally, the core apparently contained only dendrites of Forbes (1972) (Figs. 9Bl and 10Cl).

The Extreme Apex of the Preoral Section Housed the Convergence of Food and Salivary Streams With the Stylet Canals. Because of minute air pockets, the preoral section's extreme apex required special processing to visualize, and was not fully elucidated here (see Discussion). It was conical, very small, on the order of 20 μ^3, and housed the convergence of the maxillars, their consequent interlocking to form the food and salivary canals (Fig. 9Af), and the establishment of luminal continuity between these canals and the preoral foodstream lumen and salivary system,

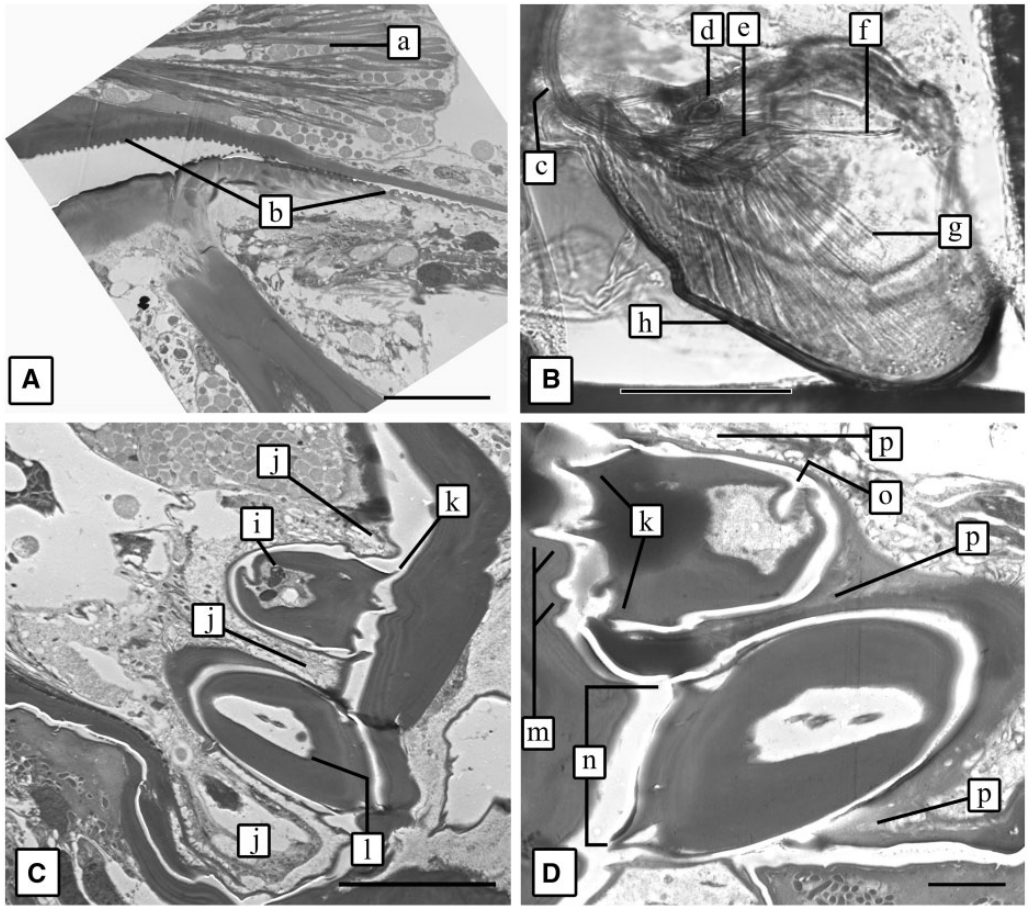

Fig. 10. Uninfected. Tentorium. **(A)** Anterior end of cibarium. Line = 2u. **(B)** Light micrograph of embedment block face, approach is parallel to the longitudinal midline. Line = 50 µ. (C) and (D) are representative sections from this block. **(C)** Preoral section. Line = 10 µ. **(D)** Corresponding section contralateral to (C), but closer to the midline. Line = 2 µ. **(a)** Salivary pump muscles. **(b)** Tanidia on inner ventral cibarial wall posteriorly, and inner dorsal (pharyngeal?) wall anteriorly. **(c)** Stylet bundle bends dorsally to enter the crumena. **(d)** Salivary pump. **(e)** Cibarium. **(f)** Esophagus. **(g)** Cuticular spatulae associated with cibarial dilator muscles (Figs. 3Cn and 6Ai). **(h)** Rostral cuticle. **(i)** Cellular core of maxillar. **(j)** Holsters retain their thin cuticular walls at this cross-sectional level. **(k)** Both maxillars have five ridges on their inner lateral surfaces at these respective cross-sectional levels. **(l)** Cellular core of mandibular with dendrites of Forbes (1972). **(m)** HW has grooves that are complementary to the opposing the maxillar ridges. **(n)** Mandibular sleeves. **(o)** Maxillar sleeve. **(p)** Holster cuticle thickens as stylets converge to the midline (cf. Fig. 9Ae).

respectively. The apposition of lateral blocks in Figure 9Ad indicated that the hypopharynx and epipharynx did not extend that far posteriorly.

The posterior-most cross-section of the holsters showed that their cuticles were thicker than those more anterior, but the holsters still maintained their semicircular embrace around the stylets (compare Fig. 6Co with Figs. 9Ae and 10Dp).

Exit From the Preoral Orifice Involved Reorientation of the Stylets so That, After Interlock, a Functional "Bundle" Was Formed With a Properly Aligned, Most-Bendable Axis. Within the apex of the preoral section, the mandibular holsters reshaped themselves so as to reorient the mandibulars to a position laterad of the interlocked maxillars (Fig. 9A, lower left inset, arrow) such that the mandibulars embraced their respective outer lateral surfaces. This configuration, with the stylets "laterolateral," rather than "dorsolateral" relative to each other, is, after interlock, called the "stylet bundle." At interlock, the four stylets of the bundle were transversely oriented relative to the long axis of the body.

Immediately distad to the rerouting of the mandibulars, there occurred a gradual 90° rotation of the stylet bundle from the laterolateral orientation so that it exited the tip of the rostrum with a dorsoventral orientation at locant (r) in Fig. 8C. In that orientation, it was able to curve, on its functionally most-bendable axis, 90° to the dorsum to enter and loop around the interior of the "crumena" (Fig. 9 and inset).

The Crumena Was a Cuticular, Sac-Like Invagination of the Cervical Cuticle. After curving dorsally, the stylet bundle passed through the "crumenal aperture" in the center of the furcasternum

(Figs. 1Bc and 2Bf), to enter the crumena (Fig. 8Cs). The stylet bundle was first appressed to the anterior side of the interior of the sac on entrance, then looped to the posterior side (Fig. 8C, arrow), exiting through the same aperture. Its exit was therefore posterior to its entrance. There was no cross-over (as in Fig. 8C, inset). The aperture occurred between the furcasternal sclerites surrounding the labial base, so that on exit, the bundle was aligned to continue directly into the labial groove.

Because the crumena was an invagination, its interior was continuous with the outside of the body, and therefore, the stylet bundle, though looped within it, was still external. The crumenal wall was thin and flexible, suggesting the cuticular physiology of an arthrodial membrane (Supp. Fig. 1 [online only]). No muscle attachments were evident.

No supportive infrastructure was apparent inside, nor on the hemocoelic side, of the crumena that might give it shape. Instead, the flat, taught shape of the crumena appeared to be the effect of tension exerted by the looping of the stylet bundle. The looping around the crumenal interior adjusted the bundle's angle 90° from its preoral orifice exit to its seat in the labial furrow.

The Foregut Was Formed by the Consolidation of Hypodermal Cells Into a Seamless Tube. In the transition from preoral to postoral sections, all panels ended as creases, leaving the hypodermal cells (Fig. 5Bo) to consolidate into a single tube to form the foregut. Identification of the mouth was problematical (see Discussion). The pharynx, technically the first organ of the foregut, had no distinct demarcation from the cibarium or the esophagus, although the luminal wall of this initial foregut section had taenidiform ridges dorsally, but not ventrally. As the chamber narrowed anteriorly, the ridges abruptly ended on the dorsal side and began on the ventral side (Fig. 10A).

Saliva Entered Into the Tentorium Through a Manifold. Each of the paired salivary glands had its own salivary duct (Fig. 5Aa; Supp. Fig. 3Ad [online only]), into which saliva was secreted for eventual injection into the host plant. The ducts coalesced into a common, "median salivary duct" (Fig. 11Ac; Supp. Fig. 3Ac [online only]). The median duct was directly attached to a "salivary pump manifold" (Fig. 11Aa; Supp. Fig. 3Ab [online only]). The manifold was recognized by its short, peg-like shape, wider in girth, and with the presence of two cell types, light and dark (Fig. 11Be; Supp. Fig. 4 [online only]). The afferent salivary lumen (Fig. 11Bd and Cd) tracked from the manifold to the salivary pump. A pair of tracheae, arising from the base of the manifold (Fig. 11Ab), was severed and fused to HW during processing (Supp. Fig. 3A [online only] inset).

The Salivary Pump Had What Appeared to be a Chambered Piston. The salivary appliance, located posteroventral to the manifold and embedded in the hypopharynx inside the tentorium (Fig. 8Ad) is called the "salivary pump," or "salivary syringe" by classical authors. It was a complex, thick-walled chamber with what appeared to be a piston wedged into a seat (Fig. 11Dg). In one TEM micrograph, curved cuticular lines gave the appearance of a spring actuated mechanism to the putative piston (Fig. 11Cg).

Discussion

Comparative anatomists, both classical and modern, are in agreement that, in the primitive insect, the clypeus, labrum, maxilla, and mandible were extraoral appendages, and the airspace they surrounded had functional significance as a "food pocket." It is variously referred to as the "intergnathal space," or "preoral cavity," bounded ventrally by the "hypopharynx," a tongue-like lobe, well known among Orthoptera, laterally by the closed mandibles and maxilla, and dorsally by the clypeolabrum. The "epipharynx" is a poorly characterized structure found in "certain insects" (Snodgrass 1935), that is attached to, or is a modification of, the inner clypeolabral surface.

Anatomists are also in agreement that, in the broader homoptera, the appressed hypopharyngeal and epipharyngeal surfaces have opposing concavities which confer a bicameral shape to the preoral cavity—a bulbous anterior half, and a narrow passageway from it to the preoral orifice (Butt 1943, Hunter *et al.* 1996:300, f. 6, Almeida and Purcell 2006:885, f. 1). The true "mouth," pharynx, and esophagus, directly follow the bulbous anterior half, and, together, make up the foregut or stomodeum. The alimentary canal starts at the mouth.

Backus and McLean (1982) gave functional characterization to a valve in the middle of the preoral cavity, between the two halves, of the sharpshooter, *Macrosteles fascifrons* Stal, and elucidated the array of gustatory dendrites that are socketed into apertures along the posterior half's length. They considered the whole preoral cavity to be the "cibarium," but gave separate distinction to the posterior half by naming it the "precibarium." Harris *et al.* (1996) asserted that in order to preserve the connotation of "cibarium" to the entire preoral cavity, both anterior and posterior sections needed to be given separate names. They proposed "antecibarium" and "postcibarium," and took the terminological diversification further by naming the dorsal cibarial half the "hypocibarium" and the ventral cibarial half the "epicibarium."

The history of the terminology for the lateral tissue blocks is more complex. Briefly, the mandibular and maxillary plates are well known structures interpreted in a wide variety of ways, by a long line of authors, to represent components of the respective appendages, modified into sclerites that gave lateral support to the stylets interior to them. Singh, one of the leading authors on homopteran oral region anatomy, presented two different line drawings, internal and external, of the Asian citrus psyllid oral region (1971:297, 299, f. 68, 69), but installed the same locants for both plates in both figures. Another locant, labeled "maxillary lever," pointed to a structure extending inward, from the envisioned maxillary plate to the maxillary stylet. In potato psyllids, the corresponding structure is the holster, which pinches away from the HW panel wall in the

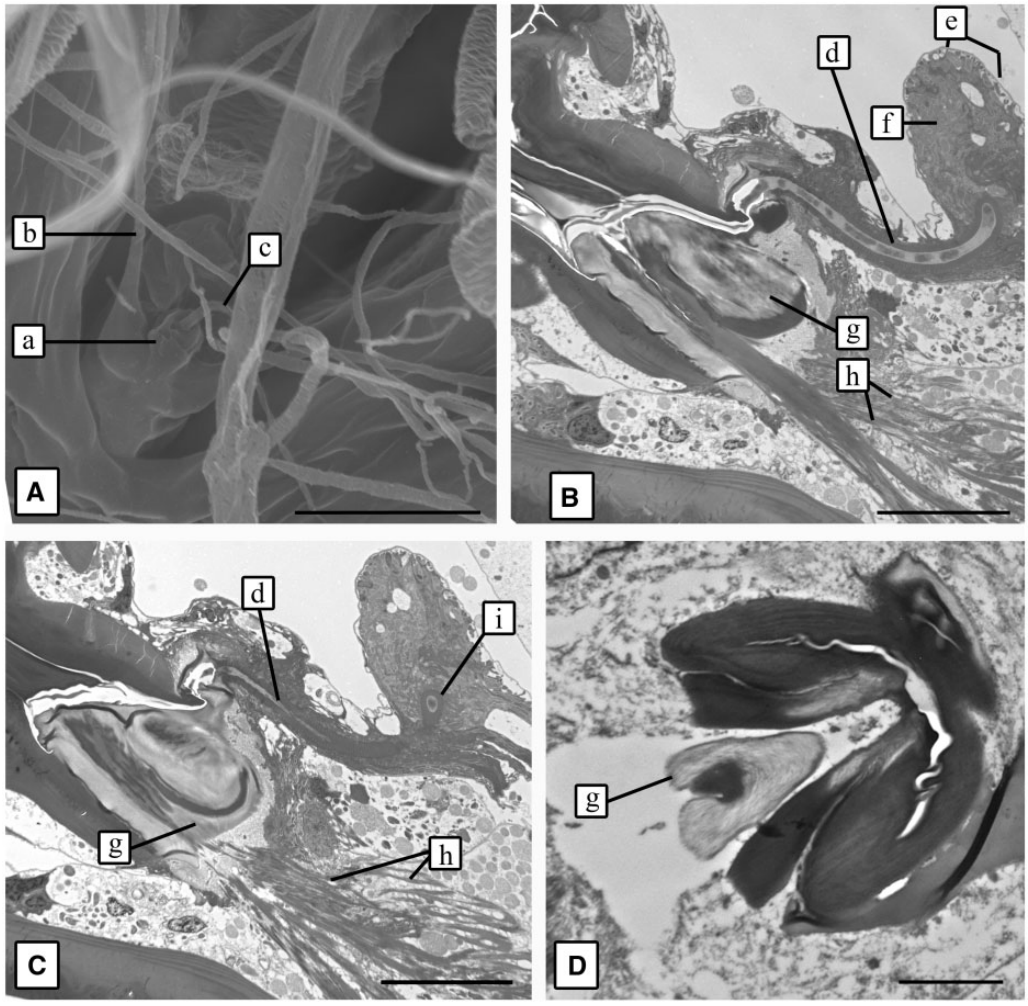

Fig. 11. Uninfected. Proximal salivary system. **(A)** SEM of salivary pump manifold. Line = 15 µ. (B) and (C) Representative sections from block in Figure 10B. **(B)** Longitudinal section of afferent salivary canal. Line = 10 µ. **(C)** A spring-like action is suggested in the salivary pump configuration. Line = 10µ. **(D)** Different specimen. Cross-section of salivary pump, dorsoventral view. Line = 2.5 µ. **(a)** Salivary pump manifold. **(b)** Trachea. **(c)** Median salivary duct. **(d)** Afferent salivary canal, from manifold to pump. **(e)** Light cytoplasm of manifold. **(f)** Dark cytoplasm of manifold. **(g)** Salivary pump. **(h)** Salivary pump muscles. **(i)** Salivary canal inside manifold. **(j)** Apparent piston wedged in the salivary pump chamber.

opposite direction, e. g. extends outward (Fig. 7Be), away from HW and the longitudinal midline, to become the loading sleeve (Fig. 7Bg and Cg). The OL–LO panel and the exoskeletal wall are separate fascia, with hemocoel in between (Liang 2013:498, f. 3A). Therefore, the plates cannot be depicted as occurring on both internal and external aspects. One might look for indications that the maxillary and mandibular plates have partially internalized, but, in potato psyllid, the OL wall diverges from the LO wall and sponsors the side-arms, then transitions into HW, which forms the hypopharynx, while LO transitions into the LH and forms the holsters. Deriving this configuration from an internalization of the plates cannot be done without modeling major rearrangements of the cell fields producing those cuticles. In short, homologizing these components is a cell biological problem. Other examples, far too detailed for this discussion, can be found in Results where generic terms are followed by their corresponding line of classical terms.

In potato psyllids, the dorsal, lateral, and ventral blocks are greatly simplified and enlarged, reducing the preoral cavity volume to the food-stream lumen and the narrow hollows continuous with it. The lateral tissue blocks, however they are evolutionarily derived, are not involved in the closure of the preoral food-stream. Instead, closure involves tight appression of the inner hypopharyngeal and epipharyngeal surfaces (Fig. 5Am, n).

Foundation for Morphological Analysis. Without a clear understanding of the anatomy and histology of the oral region, proliferation patterns of Liberibacter into the head cannot be described. Elucidating the anatomy of the oral region relies on building a new

foundation that allows for the use of generic terms so that continual rectification of the homology-based terminological system can be dispensed with as needed to maximize clarity in the current thesis. The shortcomings of this system cannot be corrected without exhaustive updating of our knowledge of the anatomy of the broader homopteran fauna to include analysis using modern techniques and instruments. Such studies have commenced (e.g., Rogers *et al.* 2002, Angelini and Kaufman 2005, Spangenberg *et al.* 2013), but are few in number.

Analysis of Anatomy.

Tentorium. There are no previous TEM studies that have identified, mapped, and given functional interpretation to the components of the tentorium. As an alternative to following its complex terminological history, it can be viewed as a quadrate arrangement of scaffolding hollows. All spaces of the preoral cavity, from the preoral orifice inward, into the deepest recesses of all the hollows, including the space of the preoral foodstream and that surrounding the holstered stylets, are continuous with the outside of the body. The entire foregut is constructed from, essentially, one continuous sheet of cells that forms a tube which invaginates deep into the body, and ends with the grafting of the esophagus into the filter chamber. Similarly, the tentorium can be viewed as one continuous sheet of cells that, starting with the preoral orifice hollow (near Fig. 8Aa), invaginates to form four branches, one for each holster, then branches further to define the shapes of the four tissue blocks.

Only two types of endoskeletal invaginations, the "apodeme" and the "apophysis" are recognized in the literature, and both function in support as well as provision for muscle attachments. They are distinguished, respectively, by whether their fasciae are open (e.g., the opposing epicuticles of the invagination are separate from each other) or closed (epicuticles are pressed together with no space between; Chapman 1971). These terms are not useful here because the hollows are far too complex, involving primary, secondary, tertiary and even quaternary furcations, and may be closed in one place and open in another. Determining the location of possible intervening closures in a hollow invagination would involve labor-intense Z-sectioning.

Preoral Section. In an attempt to simplify the complexity of the homopteran oral region, Ammar *et al.* (1994) considered the preoral section to be an extension of the foodstream and submitted that connotation of the term "foregut" should be extended to include it. This action also came under criticism for not maintaining the generally accepted principles of comparative homological nomenclature (Harris *et al.* 1996). Importantly however, recognition of the cibarium as a functional extension of the foodstream unveils, herein, a new insight on how to conceptually view preoral cross-sections, such as Figure 5A. If the four tissue blocks are to be considered derived from preoral appendages, then, regardless of the precise evolutionary changes that their cuticles underwent, it can be concluded that, with the exception of cibarial pumping action, they dispensed with the functionality of food manipulation and enlarged, collectively pressing against each other, and essentially blocking off the primitive, free airspace of the preoral cavity. That being the case, the spaces between the panels in Figure 5A did not, technically, arise as invaginations. The flats of the stylets are at about the same anteroposterior level as the mouth, indicating that their bases, as a whole, are also enclosed by the preoral components rather than invaginated into them. Terminological conundrums such as this can be alleviated by considering the hollows to be invaginations in a descriptive sense.

Salivary pump. Raine and Forbes (1971) produced the most modern analysis of the cuticular appliance (Fig. 11Bg) at the proximal end of the afferent salivary canal (Fig. 11Bd). It was termed the salivary syringe, or pump, by classical authors in association with its apparent piston-seat configuration, but pumping action has not yet been demonstrated. Other functional motifs are possible (Cicero and Brown 2012), including forward- and back-pressure regulation. The salivary pump manifold is composed of two types of cells, those with light cytoplasm and those with dark cytoplasm (Fig. 11Be, f; Supp. Fig. 4 [online only]). The same cell types were found in the salivary ducts of *Bemisia tabaci* (Gennadius) (Cicero and Brown 2012).

An efferent salivary duct was not distinguished amidst the complexity of this area. This conduit would transport saliva from the pump to the salivary canal of the stylet bundle. As the salivary canal of the stylet bundle is formed by the interlocking of maxillars, continuity between it and an efferent canal cannot be made by a seamless cuticular junction. Instead, a seal must be formed by the apex of an efferent duct with a shape that conforms to, and abuts against, the gradual convergence of the maxillars to their interlock. Alternatively, flutes might be formed at the efferent duct apex that are long enough and thin enough to insert into the interlock. The same considerations are held for continuity between the primary oral invagination and the stylet bundle's food canal. Ullman and McLean (1986:94, f. 6) identified flutes, referred to as "hypopharyngeal extensions," that sealed the gap in *Psylla pyricola* Foerster (Homoptera: Psyllidae). These were not located in potato psyllids. If present, they would occur anterior to the distal-most holster cuticle (Fig. 9A, e).

Stylet manipulation. Because the interiors of the holsters and loading sleeves are continuous with the outside of the body, the stylet bases lodged in them can have no attachment to muscles. Electropenetration graph data of psyllids (Bonani *et al.* 2010, Civolani *et al.* 2011, Butler *et al.* 2012) track the waveforms associated with specific stylet activities that are the indirect result of deformations of the lateral blocks and manipulations of the loading sleeves, caused by exertions of the muscles attached to them. Such manipulations are moderated by the cuticular cushions (Fig. 8Bq; Wensler 1974, pl. 2, f. 5, cm); the invagination corridor (the "pinch") pointed to in Figures 5Bp, 6Cq, 7Bf, and 8Ae is probably used as a fulcrum.

Forbes (1964) and Davidson (1914) indicate two pairs of lateral tissue blocks associated with the respective stylet pairs in aphids. The small, unidentified tissue block in Figure 5Bt may have comparative significance to the lower of the two pairs when elucidated. It appears from Davidson's drawings that, in Z-series, the maxillar migrates in position from a shallow holster in the upper lateral block, to the hollow between the two, then to a shallow holster in the lower lateral block.

Stylet convergence and exit. Inside the tentorium, the mandibulars are ventral to the maxillars (Fig. 10C, D), but on exit from the rostral apex, they are lateral to them (Fig. 9A). This indicates that, inside the apex of the preoral section, the mandibular holsters reshape themselves so that the mandibulars are repositioned to the outer maxillar flanks (Fig. 9A, lower inset, arrow). With this repositioning, and at the maxillar interlock, all four stylets are in laterolateral orientation relative to each other, and the bundle is, as a whole, transversely oriented. At the point of maxillar interlock, the food canal is ventral to the salivary canal, in correspondence to the foregut, similarly, ventral to the salivary pump. Upon entering and exiting the crumena, the stylets are in anteroposterior orientation relative to each other (Fig. 9B). This indicates that, on exit from the preoral orifice, the stylet bundle rotates 90°, about its longitudinal axis, from transverse to dorsoventral. With this rotation, the individual stylets are able to slide against each other as the bundle bends, perhaps 270°, to enter the crumena. Bending continues as it loops around the interior of, and exits, the crumena.

The angling of the stylet bundle in Figure 9A is interpreted as an intermediate of that rotation. It is suggested that the rotation allows the bundle to negotiate through the crumena about its most-bendable axis. If the loop was made with the stylet bundle in a transverse orientation, the arrangement would be contraindicative to the most-bendable axis and create the tendency to buckle and disengage the maxillar interlock. No studies have been found that address the relationship between the degree of interlock and the tendency to disengage when the bundle is bent against its most-bendable axis, especially during the downward pressure exerted for host plant penetration. A relationship may occur among taxa with regard to the degree of interlock and degree to which the bundle can bend against the axis without disengaging. Special reference should go to taxa that do not employ the sheath feeding strategy (Backus *et al.* 2005). The salivary sheath may, among other proposed functions (Morgan *et al.* 2013), serve to maintain interlock when the pathway of the stylet bundle angles against the most-bendable axis inside the host plant tissue.

It was noted that, proximal to the repositioning of the mandibulars to the outer lateral surface of the maxillars, the adjacent HW cuticle possessed a configuration that was complementary to the five maxillar ridges (Fig. 10Dm). These complementary grooves may assist in maintaining functional alignment and rotation during interlock. Maintenance of alignment and rotation is continued posteriorly by the partial embrace of the holster walls, which thicken in this area (Fig. 9Ae).

Postoral section. The extensions from the loading sleeves (Figs. 4Ac and 6Bm) are interpreted to be the atria of the stylet replacement organs ("retortiform organs"—Heriot 1934, Pinet 1968), and are the subject of an associated paper. Briefly, the atria are tubes of thin cuticle that house the presumptive stylets as they are formed behind the ecdysial stylets. The atria and presumptive stylets are generated by cell assemblages which, after ecdysis of the old stylets and deployment of the new stylets, return to their position as end-caps of the mandibular and maxillar (Fig. 7Cm).

The cushions (Fig. 8B) are interpreted to be the atrial walls, bunched up and compacted when the new stylets, manufactured during the prior pharate stage, are holstered into place. Cuticular continuity is expected to occur from the loading sleeve, through the bunched lamina of the cushion, to the rim of the stylet flat, across the flat, then down into, and up out of, the stylet hollow (Fig. 7Cn). The compact bunching of the cuticle probably serves to modulate stylet flexations by the manipulating muscles.

Crumena. The crumena is a cuticular, sac-like inpocketing of the exoskeleton (Figs. 2Bf and 8C), and hence comparable to other endoskeletal features such as phragma and apodemes, except for its soft, stretchable, consistency (Ullman and McLean 1986). Study of the formation of the crumena and routing of the stylet bundle into it, during ecdysis, and without an alternative looping (cf. Fig. 8C, inset) has not yet been undertaken.

The wide space of the crumenal interior, and the separation between maxillars and mandibulars in Figure 9B, are processing artifacts. Supp. Fig. 1 (online only) shows the crumenal walls to be held tightly together, which is consistent with a taut circumvention by the stylets, and with hemolymphic pressure in vivo. There is no interlock between the inner mandibular and outer maxillar faces, indicating that the surrounding crumenal cuticle, and the labial groove (Fig. 2Bg; Rosell *et al.* 1995) function to keep them tightly appressed. The crumena itself functions to reroute the stylet bundle from a posterior direction, on exit from the preoral orifice, to a ventral direction, so that the bundle can be directly inserted into the plant tissue.

Supplementary Data

Supplementary data are available at *Annals of the Entomological Society of America* online.

Acknowledgments

We thank Tony Day, David Elliott, and Steve Hernandez, The University of Arizona Spectroscopy & Imaging Facilities, for their help with microscopy, Patricia Jansma, the UA Department of Neuroscience, for consultation in the insect nervous system, and Tonja Fisher, the UA School of Plant Sciences, for versatile assistance with computer and laboratory needs. Also, Andrew McCabe and Peter Altoff, the UA Office

of Student Computing Resources, Sean van Zyl and Dean Zirwas, Graphics Design Technology, Indian River State College, Ft. Pierce, FL, for expertise in graphics design programs, and Joseph Munyaneza, USDA-ARS Wapato, WA, for supply of live psyllid colonies. This study was funded by a grant from the Florida Citrus Advanced Technology Program Project #34, Citrus Research and Development Foundation.

References Cited

Almeida, R.P.P., and A. H. Purcell. 2006. Patterns of *Xylella fastidiosa* colonization on the precibarium of sharpshooter vectors relative to transmission to plants. Ann. Entomol. Soc. Am. 99: 884–890.

Ammar, E. D., U. Järlfors, and T. P. Pirone. 1994. Association of potyvirus helper component protein with virions and the cuticle lining the maxillary food canal and foregut of an aphid vector. Phytopathology 84: 1054–1060.

Ammar, E. -D., R. G. Shatters, and D. G. Hall. 2011a. Localization of *Candidatus* Liberibacter asiaticus, associated with Citrus huanglongbing disease, in its psyllid vector using fluorescence *in situ* hybridization. J. Phytopathol. 159: 726–734.

Ammar, E. -D, R. G. Shatters, C. Lynch, and D. G. Hall 2011b. Detection and relative titer of *Candidatus* Liberibacter asiaticus in the salivary glands and alimentary canal of *Diaphorina citri* (Hemiptera: Psyllidae) vector of citrus Huanglongbing disease. Ann. Entomol. Soc. Am. 104: 526–533.

Angelini, D. R. and T. C. Kaufman. 2005. Insect appendages and comparative ontogenetics. Dev. Biol. 286: 57–77.

Backus, E. A., M. S. Serrano, and C. M. Ranger. 2005. Mechanisms of hopperburn: An overview of insect taxonomy, behavior, and physiology. Ann. Rev. Entomol. 50: 125–151.

Backus, E. A. and D. L. McLean. 1982. The sensory systems and feeding behavior of leafhoppers. I. The aster leafhopper, *Macrosteles fascifrons* Stal (Homoptera, Cicadellidae). J. Morphol. 172: 361–379.

Bonani, J. P., A. Fereres, E. Garzo, M. P. Miranda, B. Appezzato-Da-Gloria, and J.R.S. Lopes. 2010. Characterization of electrical penetration graphs of the Asian citrus psyllid, *Diaphorina citri*, in sweet orange seedlings. Entomol. Exp. Appl. 134: 35–49.

Bove, J. M. 2006. Huanglongbing: A destructive, newly-emerging, century-old disease of citrus. J. Plant Pathol. 88: 7–37.

Brlansky, R. H., and M. E. Rogers. 2007. Citrus huanglongbing: Understanding the vector-pathogen interaction for disease management. APSnet Features. December (http://www.apsnet.org/publications/apsnetfeatures/Pages/PotatoZebraChip.aspx). (accessed 27 June 2015). doi: 10:1094/APSnetFeature-2007-1207.

Brown, J. K., M. Rehman, D. Rogan, R. R. Martin, and A. M. Idris. 2010. First report of "*Candidatus* Liberibacter psyllaurous" (syn "*Ca*. L. solanacearum") associated with 'tomato vein-greening' and 'tomato psyllid yellows' diseases in commercial greenhouses in Arizona. Plant Dis. 94: 376.

Butler, C. D., G. P. Walker, and J. T. Trumble. 2012. Feeding disruption of potato psyllid, *Bactericera cockerelli*, by imidacloprid as measured by electrical penetration graphs. Entomol. Exp. Appl. 142: 247–257.

Butt, F. H. 1943. Comparative study of mouth parts of representative Hemiptera-Homoptera. Cornell Univ. Agric. Exp. Stat. Mem. 254: 1–28.

Chapman, R. F. 1971. The insects: Structure and Function, 2nd ed. Elsevier North Holland Inc., New York, NY.

Cicero, J. M. and J. K. Brown 2012. Ultrastructural studies of the salivary duct system in the whitefly vector *Bemisia tabaci* (Aleyrodidae: Hemiptera). Ann. Entomol. Soc. Am. 105: 701–717.

Civolani, S., M. Leis, G. Grandi, E. Garzo, E. Pasqualini, S. Musacchi, M. Chicca, G. Castaldelli, R. Rossi, and W. F. Tjallingii. 2011. Stylet penetration of *Cacopsylla pyri*; an electrical penetration graph (EPG) study. J. Insect Physiol. 57: 1407–1419.

Crosslin, J.M., J. E. Munyaneza, J. K. Brown, and L. W. Liefting. 2010. A history in the making: Potato zebra chip disease associated with a new psyllid-borne bacterium – a tale of striped potatoes. APSNet Features, January (http://www.apsnet.org/publications/apsnetfeatures/Pages/PotatoZebraChip.aspx). Last accessed 27 June 2015. doi:10.1094/APSnetFeature-2010-0110.

Davidson, J. 1914. On the mouth-parts and mechanism of suction in *Schizoneura lanigera*, Hausmann. J. Linn. Soc. Lond. 32: 307–332.

DuPorte, E. M. 1962. The anterior tentorial arms in insects and their significance in interpreting the morphology of the cranium of the cicadas. Can. J. Zool. 40: 137–144.

Forbes, A. R. 1964. The morphology, histology, and fine structure of the gut of the green peach aphid, *Myzus persicae* (Sulzer) (Homoptera: Aphididae). Mem. Entomol. Soc. Can. 36: 34–74.

Forbes, A. R. 1972. Innervation of the stylets of the pear psylla, *Psylla pyricola* (Homoptera: Psyllidae), and the greenhouse whitefly, *Trialeurodes vaporariorum* (Homoptera: Aleyrodidae). J. Entomol. Soc. Br. Columbia 69: 27–30.

Gottwald, T. R., J. V. da Graca, and R. B. Bassanezi. 2007. Citrus huanglongbing: The pathogen and its impact. Plant Health Prog. (http://www.plantmanagementnetwork.org/pub/php/review/2007/huanglongbing/). (accessed 27 June 2015). doi:10.1094/PHP-2007-0906-01-RV.

Hamilton, K.G.A. 1981. Morphology and evolution of the Rhynchotan head (Insecta: Hemiptera, Homoptera). Can. Entomol. 113: 953–974.

Hansen, A. K., J. T. Trumble, R. Stouthamer, and T. D. Paine. 2008. A new Huanglongbing species, "*Candidatus* Liberibacter psyllaurous," found to infect tomato and potato, is vectored by the psyllid *Bactericera cockerelli* (Sulc). Appl. Environ. Micro. 74: 5862–5865.

Harris, K. F., Z. Pesic-Van Esbroeck, and J. E. Duffus. 1996. Anatomy of a virus vector, pp. 289–318. *In* D. Gerling and R. T. Mayer (eds.). *Bemisia* 1995. Taxonomy, biology, damage control and management. Intercept Ltd. Andover, United Kingdom.

Heriot, A. D. 1934. The renewal and replacement of the stylets of sucking insects during each stadium, and the method of penetration. Can. J. Res. 11: 602–612.

Hunter, W. B., E. Hiebert, S. E. Webb, J. E. Polston, and J. H. Tsai. 1996. Precibarial and cibarial chemosensilla in the whitefly, *Bemisia tabaci* (Gennadius) (Homoptera: Aleyrodidae). Int. J. Insect Morphol. Embryol. 25: 295–304.

Jagoueix, S., J. M. Bove and M. Garnier. 1996. PCR detection of the two 'Candidatus' liberobacter species associated with greening disease of citrus. Mol. Cell. Probes 10: 43–50.

Liang, X., C. Zhang, Z. Li, L. Xu, and W. Dai. 2013. Fine structure and sensory apparatus of the mouthparts of the pear psyllid *Cacopsylla chinensis* (Yang et Li) (Hemiptera: Psyllidae). Arthropod Struct. Dev. 42: 495–506.

Liefting, L. W., Z. C. Perez-Egusquiza, and G.R.G. Clover. 2008. A new '*Candidatus* Liberibacter' species in *Solanum tuberosum* in New Zealand. Plant Dis. 92: 1474.

Liefting, L. W., P. W. Sutherland, L. I. Ward, K. L. Paice, B. S. Weir, and G.R.G. Clover. 2009. A new '*Candidatus* Liberibacter' species associated with diseases of solanaceous crops. Plant Dis. 93: 208–214.

Massonie, G., M. Garnier, and J. M. Bove. 1976. Transmission of Indian citrus decline by *Trioza erytreae* (Del Guercio),

the vector of South African Greening, pp. 18–20. *In* E. C. Calavan (ed.). Proceedings of the 7th Conference of the International Organization of Citrus Virologists. IOCV, Riverside, CA.

Morgan, J. K., G. A. Luzio, E. D. Ammar, W. B. Hunter, D. G. Hall, and R. G. Shatters Jr. 2013. Formation of stylet sheaths *in āere* (in air) from eight species of phytophagous hemipterans from six families (Suborders: Auchenorrhyncha and Sternorrhyncha). PLoS ONE 8: e62444.

Munyaneza, J. E., J. M. Crosslin, and J. E. Upton. 2007. Association of *Bactericera cockerelli* (Homoptera: Psyllidae) with "zebra chip", a new potato disease in southwestern United States and Mexico. J. Econ. Entomol. 100: 656–663.

Pinet, J. M. 1968. Structure et formation des coaptations des stylets maxillaires de *Rhodnius prolixus* (Heter. Reduviidae). Ann. Soc. Entomol. Fr. (N.S.). 4: 455–475.

Raine, J. and A. R. Forbes. 1971. The salivary syringe of the leafhopper *Macrosteles fascifrons* (Homoptera: Cicadellidae) and the occurrence of mycoplasma-like organisms in its ducts. Can. Entomol. 103: 110–116.

Rogers, B.T., M.D. Peterson, and T.C. Kaufman. 2002. The development and evolution of insect mouthparts as revealed by the expression patterns of gnathocephalic genes. Evol. Dev. 4: 96–110.

Rosell, R. C., J. E. Lichty, and J. K. Brown. 1995. Ultrastructure of the mouthparts of adult sweetpotato whitefly, *Bemisia tabaci* Gennadius (Homoptera: Aleyrodidae). Int. J. Insect Morphol. Embryol. 24: 297–306.

Sambrook, J., E. F. Fritsch, and T. Maniatis. 1989. Molecular cloning: A laboratory manual, 2nd ed. Cold Spring Harbor Laboratory Press, New York, NY.

Singh, S. 1971. Morphology of the head of Homoptera. Res. Bull. Panjab Univ. Sci. 22: 261–316.

Snodgrass, R. E. 1935. Principles of insect morphology, 1st ed. McGraw-Hill Book Co., New York, NY.

Spangenberg, R., K. Friedemann, C. Weirauch, and R. G. Beutel. 2013. The head morphology of the potentially basal heteropteran lineages Enicocephalomorpha and Dipsocoromorpha (Insecta: Hemiptera: Heteroptera). Arthropod Syst. Phyl. 71: 103–136.

Ullman, D. and D. L. McLean. 1986. Anterior alimentary canal of the pear psylla, *Psylla pyricola* Foerster (Homoptera, Psyllidae). J. Morphol. 189: 89–98.

Weber, H. 1929. Kopf und thorax von *Psylla mali* Schmidb. (Hemiptera-Homoptera.) Eine morphogenetische studie. Zeitschr. F. Morphol. U. Okol. D. Tiere. 14: 59–165.

Wensler, R. J. D. 1974. Sensory innervation monitoring movement and position in the mandibular stylets of the aphid, *Brevicoryne brassicae*. J. Morphol. 143: 349–364.

Received 1 October 2014; accepted 15 June 2015.